An energy-saving optimization method for robot laser welding systems based on multi-objective metaheuristic algorithms

Jin Zhou[1], Pei Jiang[2], Chongfu Huang[3], Kehan Ping[4]
[1, 3]School of Intelligent Manufacturing and Transportation, Chongqing Vocational Institute of Engineering, Chongqing, China
[1, 2, 4]State Key Laboratory of Mechanical Transmission, Chongqing University, Chongqing, China
[3]Corresponding author
E-mail: [1]*zhoujin@cqvie.edu.cn*, [2]*Peijiang@cqu.edu.cn*, [3]*hcf1996@cqvie.edu.cn*, [4]*202107131132t@stu.cqu.edu.cn*

Received 11 July 2024; accepted 10 January 2025; published online 27 February 2025
DOI https://doi.org/10.21595/jme.2025.24349

Abstract. Reducing the energy consumption of robot manufacturing systems has become one of the increasingly important issues in industry. However, for robot manufacturing systems, the traditional optimization method with energy consumption as the objective function always suffers from low efficiency. In view of this, a novel energy-saving optimization method is proposed for robot laser welding systems based on the multi-objective optimization in this paper. This method deconstructs the energy consumption objective into three computationally inexpensive feature objectives and uses these three feature objectives as the objective functions of optimization, thus significantly improving the optimization efficiency. And a comprehensive optimization model of robot laser welding systems, which simultaneously considers three factors: the layout pose of workpieces, the posture of laser tools, and the inverse kinematics solution of robots, is established by utilizing a task energy characteristic model based on the time-scaling method. Furthermore, an integrated optimization process based on the NSGA-II algorithm is presented. A case study is described in detail. The results of the case study demonstrate that the proposed optimization method leads to a remarkable increase of over 95 % in optimization efficiency, that three factors exhibit interdependence, and that the integrated optimization of these factors yields superior results compared to optimizing them individually. In the case study, at a 95 % confidence level, the optimization scheme reduces the energy consumption of idle motion by 34.91 % and the total energy consumption by 7.29 %, compared to the original scheme.

Keywords: industrial robot, laser welding, energy saving, multi-objective optimization, and metaheuristic algorithm.

1. Introduction

In contemporary manufacturing, industrial robots have emerged as indispensable assets due to its exceptional flexibility, extensive working range, and cost-effectiveness [1], [2]. As of 2022, over 3.5 million industrial robots were in use across global factories. [3]. However, the widespread adoption of industrial robots also presents a significant challenge: an inevitable increase in energy consumption. Currently, reducing the energy consumption of robotic manufacturing systems has become a paramount priority, as it is crucial for achieving sustainable manufacturing and mitigating the impact of rising energy costs [4], [5].

Numerous scholars have conducted extensive research on energy-saving techniques of industrial robots, encompassing task allocation [6], operation scheduling [7], processing parameter optimization [8], path optimization [9], trajectory optimization [10], etc. And the energy consumption prediction of industrial robots is the basis of these techniques. Among these techniques, the energy-saving trajectory planning is one of main aspects [11]. Vergnano et al. [12] establish a parameterized energy consumption model of industrial robots and schedule the

trajectory to minimize energy consumption based on a time-scaling method. The time-scaling method has garnered significant attention due to its capability to optimize trajectories in the time domain and efficiently predict energy consumption [7], [13]-[16].

However, this method does not modify the motion path of the end tool and the robotic configurations in the spatial domain. Therefore, the minimum energy consumption obtained by this method specifically belongs to the specified motion path of the end tool and the specified robotic configurations. And, according to robotic kinematics, the motion path of the end tool and the robotic configurations are influenced by the layout pose of workpieces, the posture of the end tool, and the inverse kinematics solutions of 6-axis robots at each path point (The inverse kinematics of 6-axis robots yields eight possible solutions at each path point of the end tool). Therefore, modifying these three factors aforementioned will affect the minimum energy consumption obtained by the time-scaling method.

Optimizing these three factors represents a significant energy-saving approach for robotic manufacturing systems. Gadaleta et al. [17] achieved a reduction in energy consumption of robots by 16.4 % through optimizing the layout position of workpieces. Feng et al. [18] achieved a 10.33 % reduction in robotic energy consumption by flexibly selecting robotic inverse kinematics solutions for cyclic pick-and-place tasks. However, prior studies have predominantly focused on the impact of individual factors and have not adequately considered the interplay among these three factors and their comprehensive effects.

Robot laser welding technology has found extensive applications in diverse manufacturing industries [19]-[23]. Nevertheless, laser welding is characterized by high energy consumption and low energy efficiency [24]. Furthermore, the power consumption of laser devices and auxiliary chillers is significant and exerts a substantial impact on the energy consumption characteristics and optimization features of robot laser welding systems [20]. Therefore, it is necessary to optimize the overall energy consumption of such systems by taking into account the system-level energy consumption characteristics. However, current research on energy-saving optimization of robot laser welding systems, particularly for the welding of complex components, remains limited.

Therefore, this paper systematically investigates the energy-saving method for robotic laser welding of complex components by leveraging the functional redundancy of the robot, while effectively addressing the associated optimization challenges. The main contributions are as follows: 1) Through deconstructing the energy consumption objective, a novel energy-saving optimization method is proposed for robot laser welding systems based on multi-objective optimization. 2) A comprehensive optimization model, which simultaneously incorporates three factors, is developed for the robot laser welding system.

2. Description and modeling of the problem

2.1. Description of the problem

A typical robot laser welding system primarily consists of an industrial robot, a laser, and a chiller, as shown in Fig. 1. Fig. 1 additionally illustrates a case of workpiece welding utilizing the robotic laser welding system. $\{CS_0\}$ denotes the coordinate system of the robot base, $\{CS_{Tool}\}$ represents the tool coordinate system, and $\{CS_W\}$ signifies the workpiece coordinate system. The robot's motion from one stationary point to the next is defined as a sub-motion, which can be programmed using a standard robot motion instruction, during the workpiece welding process. Based on the operational state of the laser, the sub-motion is categorized into two types: the welding sub-motion and the idle sub-motion.

In reference [20], we have studied the characteristics and modeling of energy consumption in robot laser processing systems in detail and analyzed energy-saving approaches for the processing of complex parts. For a given workpiece, the energy consumption and execution time of welding sub-motions are primarily determined by the planned welding process parameters, which remain invariant throughout the welding procedure. However, it is important to note that the minimum

energy consumption and execution time for each idle sub-motion, obtained through the time-scaling method under given constraints, are closely related to the layout pose of workpieces in $\{CS_0\}$, the posture of the laser tool along the tool center point's motion path, and the inverse kinematics solutions of 6-axis robots at each path point of the end tool. A typical case is illustrated in Fig. 19 of reference [20]. In this case, the energy consumption of idle sub-motions under four different scenarios exhibits a difference of 42.13 % between the minimum and maximum values. Therefore, optimizing these three factors can significantly reduce the energy consumption of idle sub-motions during the welding of a workpiece.

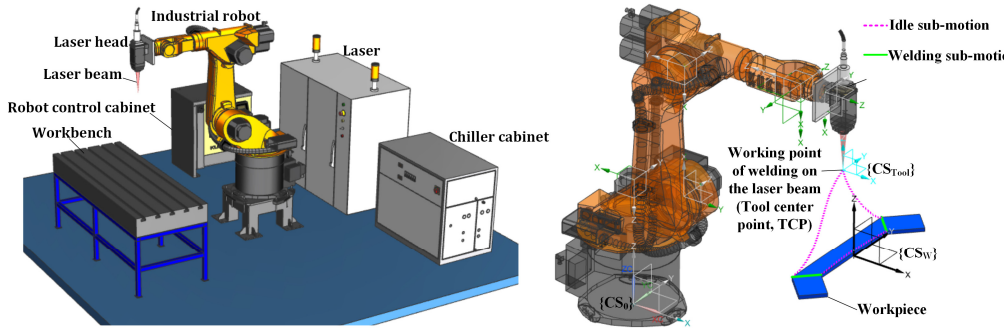

Fig. 1. The basic set-up of a typical robot laser welding system and a case of workpiece welding

Furthermore, to illustrate how these three factors influence the minimum energy consumption of idle sub-motions obtained through the time-scaling method under constraints, the example of the linear path task in Fig. 18 of reference [20] is utilized. The energy consumption is calculated using the model established in reference [20], and the calculation result of the total energy consumption of the robot laser welding system (represented by the red solid line) is plotted in the figure. The new figure is designated as Fig. 2. In Fig. 2, EC represents the energy consumption, IR represents the industrail robot, and RLWS represents the robot laser welding system. $T_{\min}$ represents the minimum execution time of the linear path task while satisfying kinematic constraints, $T_{\mathrm{E-opt,RLWS}}$ represents the energy-optimal time of the RLWS, and $T_{\mathrm{E-opt,robot}}$ represents the energy-optimal time of the robot.

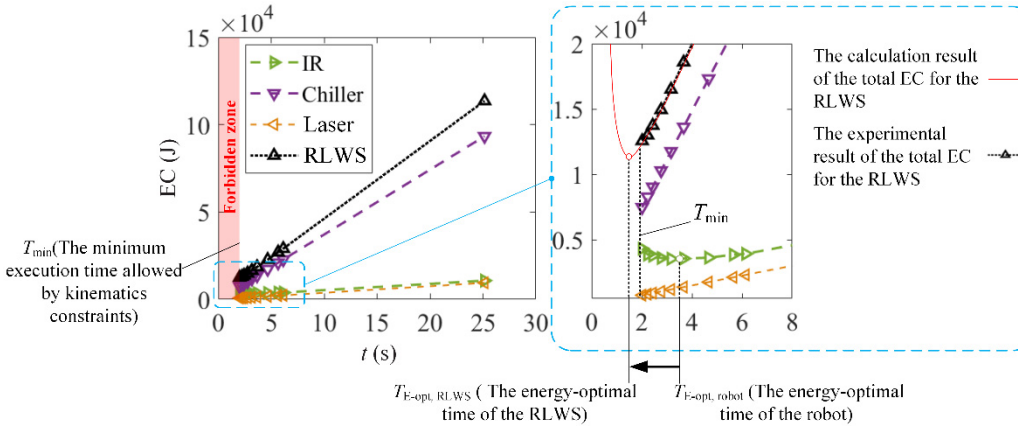

Fig. 2. The changes of the energy consumption of each subsystem and the total energy consumption with execution time

As illustrated in Fig. 2, the huge power consumption of the laser and the chiller results in the $T_{\mathrm{E-opt,RLWS}}$ being smaller than $T_{\min}$; obviously, a shorter execution time for tasks can lead to a

reduction in overall system energy consumption. If the layout pose of workpieces, the posture of laser tools, and the inverse kinematics solution of robots are unreasonable, the corresponding $T_{\min}$ will be large, thus resulting in a high energy consumption. Therefore, optimizing these three factors to effectively reduce the energy consumption of idle sub-motions is a critical energy-saving strategy for robot laser processing systems. Next, a comprehensive mathematical model will be developed.

2.2. Problem modeling

Assume that a workpiece with N_{weld} welding seams needs to be processed, and there are N_{idle} non-welding strokes during the processing. According to [12], when the reference trajectory is pre-planned, the energy consumption of each sub-motion can be expressed as a polynomial function with respect to execution time, known as the task energy characteristic model, based on the time-scaling method. The minimum energy consumption (E'_{idle}) of idle sub-motions, which is obtained by the time-scaling method under constraints, can be expressed as follows [20]:

$$E'_{\text{idle}} = \sum_{j=1}^{N_{\text{idle}}} \left[\begin{array}{l} \left(P_{\text{LD\_pre}} + \bar{P}_{\text{cool}} + \mu'_{0,\text{idle},j}\right) T'_{\text{idle},j} + \mu'_{1,\text{idle},j} + \mu'_{2,\text{idle},j} \dfrac{1}{T'_{\text{idle},j}} \\ + \mu'_{3,\text{idle},j} \dfrac{1}{{T'_{\text{idle},j}}^2} + \mu'_{4,\text{idle},j} \dfrac{1}{{T'_{\text{idle},j}}^3} \end{array} \right], \tag{1}$$

$$T'_{\text{idle},j} = \max \left\{ \begin{array}{l} T_{\min,\text{idle},j}\left(Pose_{\text{w}}, Posture_{\text{tool}}^{j,1}, \cdots, Posture_{\text{tool}}^{j,N_{\text{tool}}}, IKS^{j,1}, \cdots, IKS^{j,N_{\text{tool}}}\right), \\ T_{\text{E-opt},\text{idle},j}\left(Pose_{\text{w}}, Posture_{\text{tool}}^{j,1}, \cdots, Posture_{\text{tool}}^{j,N_{\text{tool}}}, IKS^{j,1}, \cdots, IKS^{j,N_{\text{tool}}}\right) \end{array} \right\}, \tag{2}$$

where N_{idle} represents the number of idle sub-motions, the polynomial coefficients $\mu'_{0,\text{idle},j}$, $\mu'_{1,\text{idle},j}$, $\mu'_{2,\text{idle},j}$, $\mu'_{3,\text{idle},j}$, $\mu'_{4,\text{idle},j}$ are the task energy consumption coefficients of the j-th idle sub-motion. Further details of the polynomial coefficients are provided by Eqs. (13-34) in reference [20]. $P_{\text{LD\_pre}}$ is the input power of lasers in the lasing-preparation state, $\bar{P}_{\text{cool}}$ is the average power of the chiller. $T'_{\text{idle},j}$ is the execution time corresponding to minimum energy consumption of the j-th idle sub-motion under constraints, and $T_{\min,\text{idle},j}$ is the minimum execution time of the j-th idle sub-motion with satisfying constraints. $T_{\text{E-opt},\text{idle},j}$ is the energy-optimal time of the j-th idle sub-motion. $Pose_{\text{w}}$ represents the workpiece layout pose. $Posture_{\text{tool}}^{j,i}$ (i = 1, …, N_{tool}) and $IKS^{j,i}$ represent the tool posture and the inverse kinematics solution of robots at the sampling point i along the j-th idle sub-motion path curve, respectively. N_{tool} is the sampling point number.

Based on the methodology for rigid body pose description, $Pose_{\text{w}}$ can be represented by six variables: x_{w}, y_{w}, z_{w}, θ_{C}, θ_{B}, and θ_{A}. θ_{C}, θ_{B}, and θ_{A} are the rotational angles of $\{\text{CS}_{\text{W}}\}$ about the X, Y, and Z axes of $\{\text{CS}_0\}$, respectively, which describe the posture of the workpiece in $\{\text{CS}_0\}$. $(x_{\text{w}}, y_{\text{w}}, z_{\text{w}})^T$ is the position vector of the origin of $\{\text{CS}_{\text{W}}\}$ in $\{\text{CS}_0\}$, describing the position of the workpiece in $\{\text{CS}_0\}$. Similarly, the laser tool pose in $\{\text{CS}_{\text{W}}\}$ can be represented by six variables: x, y, z, C, B, and A. C, B, and A represent the rotational angles of $\{\text{CS}_{\text{Tool}}\}$ about the X, Y, and Z axes of $\{CS_W\}$, respectively, which describe the laser tool posture in $\{\text{CS}_{\text{W}}\}$. $(x, y, z)^T$ is the position vector of the origin of $\{\text{CS}_{\text{Tool}}\}$ (namely the tool centre point) in $\{\text{CS}_{\text{W}}\}$, which represents the position of the laser tool in $\{\text{CS}_{\text{W}}\}$.

For a specified workpiece, the target positions that the tool centre point (TCP) of the laser tool needs to achieve in $\{\text{CS}_{\text{W}}\}$ are specific. However, at each target position, the posture of the laser tool can be adjusted. Moreover, for a given pose of the laser tool, the inverse kinematics of robots have eight possible solutions ($\boldsymbol{q}^{\#1}$, $\boldsymbol{q}^{\#2}$, $\boldsymbol{q}^{\#3}$, $\boldsymbol{q}^{\#4}$, $\boldsymbol{q}^{\#5}$, $\boldsymbol{q}^{\#6}$, $\boldsymbol{q}^{\#7}$, $\boldsymbol{q}^{\#8}$), which are automatically numbered during the solving process. However, optimizing the posture of laser tools and the inverse kinematic solution at each target point of continuous path motion will introduce countless

decision variables. Therefore, only the postures of laser tools and the inverse kinematic solutions at the starting and ending points of continuous path motion are considered, thus ensuring a reasonable number of decision variables.

Therefore, for the problem of optimizing the minimum energy consumption of robot laser welding systems obtained by the time-scaling method, the decision variable set is $\{x_{\mathrm{w}}, y_{\mathrm{w}}, z_{\mathrm{w}}, \theta_{\mathrm{A}}, \theta_{\mathrm{B}}, \theta_{\mathrm{C}}, A_{j,\mathrm{s}}, B_{j,\mathrm{s}}, C_{j,\mathrm{s}}, A_{j,\mathrm{e}}, B_{j,\mathrm{e}}, C_{j,\mathrm{e}}, cf_{j,\mathrm{s}}, cf_{j,\mathrm{e}} | j = 1, \ldots, N_{\mathrm{idle}}\}$. $(A_{j,\mathrm{s}}, B_{j,\mathrm{s}}, C_{j,\mathrm{s}})$ and $(A_{j,\mathrm{e}}, B_{j,\mathrm{e}}, C_{j,\mathrm{e}})$ are the attitude angles of the laser tool at the starting and ending points of the j-th idle sub-motion, respectively. $cf_{j,\mathrm{s}}$ and $cf_{j,\mathrm{e}}$ are the decision variables of inverse kinematic solutions at the starting and ending points, respectively. The general mathematical model can be expressed as follows:

$$\min \quad E'_{\mathrm{idle}} = E\left(x_{\mathrm{w}}, y_{\mathrm{w}}, z_{\mathrm{w}}, \theta_{\mathrm{A}}, \theta_{\mathrm{B}}, \theta_{\mathrm{C}}, \cdots, A_{j,\mathrm{s}}, B_{j,\mathrm{s}}, C_{j,\mathrm{s}}, cf_{j,\mathrm{s}}, A_{j,\mathrm{e}}, B_{j,\mathrm{e}}, C_{j,\mathrm{e}}, cf_{j,\mathrm{e}}, \cdots\right), \quad j = 1,2, \ldots, N_{\mathrm{idle}}, \tag{3}$$

$$s.t. \quad \begin{array}{l} x_{\mathrm{w,min}} \le x_{\mathrm{w}} \le x_{\mathrm{w,max}}, \quad y_{\mathrm{w,min}} \le y_{\mathrm{w}} \le y_{\mathrm{w,max}}, \quad z_{\mathrm{w,min}} \le z_{\mathrm{w}} \le z_{\mathrm{w,max}}, \\ \theta_{\mathrm{A,min}} \le \theta_{\mathrm{A}} \le \theta_{\mathrm{A,max}}, \quad \theta_{\mathrm{B,min}} \le \theta_{\mathrm{B}} \le \theta_{\mathrm{B,max}}, \quad \theta_{\mathrm{C,min}} \le \theta_{\mathrm{C}} \le \theta_{\mathrm{C,max}}, \end{array} \tag{4}$$

$$\begin{array}{l} A_{j,\mathrm{s,min}} \le A_{j,\mathrm{s}} \le A_{j,\mathrm{s,max}}, \quad B_{j,\mathrm{s,min}} \le B_{j,\mathrm{s}} \le B_{j,\mathrm{s,max}}, \quad C_{j,\mathrm{s,min}} \le C_{j,\mathrm{s}} \le C_{j,\mathrm{s,max}}, \\ A_{j,\mathrm{e,min}} \le A_{j,\mathrm{e}} \le A_{j,\mathrm{e,max}}, \quad B_{j,\mathrm{e,min}} \le B_{j,\mathrm{e}} \le B_{j,\mathrm{e,max}}, \quad C_{j,\mathrm{e,min}} \le C_{j,\mathrm{e}} \le C_{j,\mathrm{e,max}}, \\ j = 1, \ldots, N_{\mathrm{idle}}, \end{array} \tag{5}$$

$$cf_{j,\mathrm{s}}, \ cf_{j,\mathrm{e}} \in \{\#1, \#2, \ldots, \#8\}, \quad j = 1, \ldots, N_{\mathrm{idle}}, \tag{6}$$

$$q_{i,\mathrm{min}} \le q_i \le q_{i,\mathrm{max}}, \quad \forall i = 1, \cdots, 6, \tag{7}$$

$$|\dot{q}_i| \le V_{\mathrm{lim}}^{(i)}, \quad |\ddot{q}_i| \le A_{\mathrm{lim}}^{(i)}, \quad |\dddot{q}_i| \le J_{\mathrm{lim}}^{(i)}, \quad \forall i = 1, \cdots, 6, \tag{8}$$

$$\dot{x} \le V_{\mathrm{lim}}, \quad |\ddot{x}| \le A_{\mathrm{lim}}, \quad |\dddot{x}| \le J_{\mathrm{lim}}, \tag{9}$$

$$\sum_{j=1}^{N_{idle}} T'_{\mathrm{idle},j} \le T_{\mathrm{idle\_lim}}, \tag{10}$$

where Eqs. (4-5) address the basic constraints of workspace and laser tool postures. Since the robotic workspace is a non-ideal cube, the flexibility outside the flexible space is limited, and the intricate spatial interferences exist, any alteration in x_{w}, y_{w}, z_{w}, θ_{A}, θ_{B}, θ_{C}, $A_{j,\mathrm{s}}$, $B_{j,\mathrm{s}}$, $C_{j,\mathrm{s}}$, $A_{j,\mathrm{e}}$, $B_{j,\mathrm{e}}$, or $C_{j,\mathrm{e}}$ will inevitably lead to variations in the feasible domains of other variables. Therefore, the setting values for parameters $x_{\mathrm{w,min}}$, $y_{\mathrm{w,min}}$, $z_{\mathrm{w,min}}$, $\theta_{\mathrm{A,min}}$, $\theta_{\mathrm{B,min}}$, $\theta_{\mathrm{C,min}}$, $A_{j,\mathrm{s,min}}$, $B_{j,\mathrm{s,min}}$, $C_{j,\mathrm{s,min}}$, $A_{j,\mathrm{e,min}}$, $B_{j,\mathrm{e,min}}$, $C_{j,\mathrm{e,min}}$, $x_{\mathrm{w,max}}$, $y_{\mathrm{w,max}}$, $z_{\mathrm{w,max}}$, $\theta_{\mathrm{A,max}}$, $\theta_{\mathrm{B,max}}$, $\theta_{\mathrm{C,max}}$, $A_{j,\mathrm{s,max}}$, $B_{j,\mathrm{s,max}}$, $C_{j,\mathrm{s,max}}$, $A_{j,\mathrm{e,max}}$, $B_{j,\mathrm{e,max}}$, and $C_{j,\mathrm{e,max}}$ are redundant. The purpose is to encompass all feasible domains of the corresponding variables. Due to the dependence of the space required for processing a workpiece on the geometric shape and size of the tool, it cannot be ensured that the space required will entirely fall within the robotic workspace, even if the workpiece is located within the robotic workspace. Therefore, satisfying Eqs. (4-5) does not guarantee the attainability of all processing poses. Eq. (7) represents the joint position constraints. If there exists at least one inverse solution that satisfies all the joint position constraints for a processing pose, then the processing pose is deemed reachable; otherwise, it is deemed unreachable. Eq. (8) represents the constraints of joint velocities, accelerations, and jerks. Eq. (9) describes the limitations of the tool velocity, acceleration, and jerk. Eq. (10) signifies the constraint of processing time.

3. Solution approach based on multi-objective metaheuristic algorithms

3.1. Objective function deconstruction based on system energy consumption characteristics

The calculation of Eq. (1) is highly time-consuming due to the requirement for intricate 6-axis robot dynamics calculations during the optimization process. Therefore, this paper deconstructs the energy consumption objective into multiple feature objectives, which are computationally

efficient, based on the characteristics and key influencing factors of energy consumption of robot laser welding systems. Then, the single-objective optimization of energy consumption is transformed into a multi-objective optimization of these feature objectives. Finally, we will only compute the energy consumption of the Pareto optimal solutions resulting from multi-objective optimization, to identify the solution with the lowest energy consumption.

We conducted a detailed study on the energy consumption characteristics of a typical robot laser welding system, which forms the basis for the deconstruction of energy consumption objectives in this paper. The key analyses are presented as follows:

1) During the idle sub-motion, because the total power of the laser and the chiller is still very large, the energy-optimal point of the energy characteristic curve for the whole system is still significantly shifted to the left compared to the robot, as depicted in Fig. 2. The results indicate that, for the idle sub-motion, the energy consumption of the whole system is positively correlated with execution time to a large extent. Therefore, the idle motion time is a very important feature objective.

2) In addition, on the right side of the energy-optimal point, the smaller the time is, the smaller the rate of energy consumption reduction is. Therefore, it is always hoped that the speed of each idle sub-motion is as high as possible, while also being as close as possible, to save energy through fully utilizing the energy consumption optimization features of the system.

3) Moreover, for a specified task, robotic energy consumption is not only related to execution time, but also strongly related to the angle of joint rotation. The total joint rotation angle directly reflects the energy consumption coefficients of the task. And the larger the energy consumption coefficients are, the higher the overall energy consumption of the robot is. Therefore, the total joint rotation angle of idle motion is also an important feature objective. Considering that the energy consumption of the unit angle of each joint is different, a weighted sum is generally used.

Therefore, this paper replaces the energy consumption objective with the total time (f_{t}) of idle sub-motions, the weighted sum (f_{θ}) of joint rotation angles in all idle sub-motions, and the maximum difference ($f_{\dot{\mathrm{q}}}$) among the speeds of idle sub-motions, as the criteria to determine the individual performance in the optimization process. The equivalent joint velocity ($\bar{\dot{q}}_{\mathrm{idle},j}$, $j = 1,\ldots, N_{\mathrm{idle}}$), obtained by dividing the weighted sum of joint rotation angles by the motion time, is used for each idle sub-motion. Finally, only the energy consumption of individuals in the Pareto set, which are found through multi-objective optimization, is calculated, thus greatly reducing the calculation amount required for the energy consumption optimization process. The new objective function formulas are as follows:

$$\begin{cases} f_{\mathrm{t}} = \sum_{j=1}^{N_{\mathrm{idle}}} T'_{\mathrm{idle},j}, \\ f_{\theta} = \sum_{i=1}^{6} \omega_i \theta_i, \\ f_{\dot{\mathrm{q}}} = \max\left(\bar{\dot{q}}_{\mathrm{idle},1}, \cdots, \bar{\dot{q}}_{\mathrm{idle},N_{\mathrm{idle}}}\right) - \min\left(\bar{\dot{q}}_{\mathrm{idle},1}, \cdots, \bar{\dot{q}}_{\mathrm{idle},N_{\mathrm{idle}}}\right), \end{cases} \tag{11}$$

$$\bar{\dot{q}}_{\mathrm{idle},j} = \frac{\sum_{i=1}^{6} \omega_i \theta_{\mathrm{idle},j,i}}{T'_{\mathrm{idle},j}}, \quad \forall j \in \{1,2,\ldots,N_{\mathrm{idle}}\}, \tag{12}$$

where θ_i is the rotation angle of joint i in all idle sub-motions, ω_i is the corresponding weight value of joint i. The weight value of each joint is obtained by the Analytic Hierarchy Process method [25].

3.2. NSGA-II algorithm for optimizing the energy consumption of robot laser welding systems

The NSGA-II algorithm proposed by Deb et al. [26] has both good distribution and fast convergence rate, while it is widely used by scholars at home and abroad for multi-objective optimization problems. The NSGA-II algorithm with an elite strategy is very suitable for solving the problem in this paper.

Different robot poses have different eight inverse kinematic solutions and the amount and sequence number of feasible inverse kinematic solutions are also different. Therefore, the solution of the entire problem is divided into two parts: the basic solution, composed of decision variables $\{x_{\mathrm{w}}, y_{\mathrm{w}}, z_{\mathrm{w}}, \theta_{\mathrm{A}}, \theta_{\mathrm{B}}, \theta_{\mathrm{C}}, A_{j,\mathrm{s}}, B_{j,\mathrm{s}}, C_{j,\mathrm{s}}, A_{j,\mathrm{e}}, B_{j,\mathrm{e}}, C_{j,\mathrm{e}}, cf_{j,\mathrm{s}}, cf_{j,\mathrm{e}} | j = 1,\ldots, N_{\mathrm{idle}}\}$ of the workpiece layout pose and laser tool posture, and the subordinate solution composed of decision variables $\{cf_{j,\mathrm{s}}, cf_{j,\mathrm{e}} | j = 1,\ldots, N_{\mathrm{idle}}\}$ of eight inverse kinematic solutions at the starting and ending points of all idle sub-motions.

The optimization of the basic solution is used as the main loop. Because the basic solution is only obtained under the basic workspace constraint (4) and the laser tool posture constraint (5), it cannot be guaranteed that all processing poses, which are determined by the workpiece layout pose satisfying constraints (4) and the laser tool posture satisfying constraints (5), are reachable. For each basic solution, the reachability of each processing pose should be firstly judged to determine whether it is feasible. The basic solution with unreachable processing poses is called an unreachable solution, while the set of unreachable solutions is directly used as the worst non-dominated level.

For a basic solution which satisfies the accessibility constraint, it is necessary to determine the corresponding subordinate solution. The method is as follows: firstly, based on the three feature objectives in Eq. (11), the NSGA-II algorithm is used to obtain a set of Pareto-optimal solutions about the selection of eight inverse kinematic solutions at the starting and ending points of each sub-motion; then, the Analytic Hierarchy Process method is used to select a satisfactory solution from the Pareto set obtained as the subordinate solution corresponding to the basic solution. This process is called configuration decision-making. In the configuration decision-making, the following method is used to dimensionless three objectives. Let $Unit_{i,j}$ represent the dimensionless value of the objective j (j can be taken as f_{t}, f_{θ}, and $f_{\dot{\mathrm{q}}}$) corresponding to the Pareto-optimal solution i, and then the following function is defined:

$$Unit_{i,j} = \frac{f_{j\max} - f_{i,j}}{f_{j\max} - f_{j\min}}, \tag{13}$$

$$f_{j\max} = \max\{f_{1,j}, \cdots, f_{i,j}, \cdots, f_{N_{\mathrm{Pa}},j}\}, \quad f_{j\min} = \min\{f_{1,j}, \cdots, f_{i,j}, \cdots, f_{N_{\mathrm{Pa}},j}\}, \tag{14}$$

where $f_{i,j}$ is the function value of the objective j of the Pareto-optimal solution i, N_{Pa} is the number of Pareto-optimal solutions.

Fig. 3 shows the integrated optimization process based on the NSGA-II algorithm. Gen is the current number of iterations. N_{ite} is the maximum number of iterations. $\mathbf{P}_0$ and $\mathbf{Q}_0$ are the initial parent and offspring population of the basic solution, respectively. $\mathbf{P}_{\mathrm{t}}$ and $\mathbf{Q}_{\mathrm{t}}$ are the contemporary parent and offspring population of the basic solution, respectively. $\mathbf{R}_{\mathrm{t}}$ is the combined population of $\mathbf{P}_{\mathrm{t}}$ and $\mathbf{Q}_{\mathrm{t}}$. $\mathbf{P}_{\mathrm{t+1}}$ and $\mathbf{Q}_{\mathrm{t+1}}$ are the new parent and offspring population of the basic solution, respectively. $\boldsymbol{\mathcal{F}}_{\mathrm{k}}$ is the non-dominated level obtained by the k-th fast non-dominated sorting. The dominant relationship adopted is that if individual U and individual V meet any of the following conditions, then individual U dominates individual V:

1) Individual U satisfies all constraints while individual V does not.

2) Both individual U and individual V meet the accessibility constraint, but each objective function value of individual U is not bigger than the corresponding value of individual V and at least one objective function value is less than the corresponding value of individual V.

3) Individual U satisfies the accessibility constraint, while individual V does not satisfy the accessibility constraint.

4) Both individual U and individual V do not satisfy the accessibility constraint, but the unreachable points of individual U are less than those of individual V.

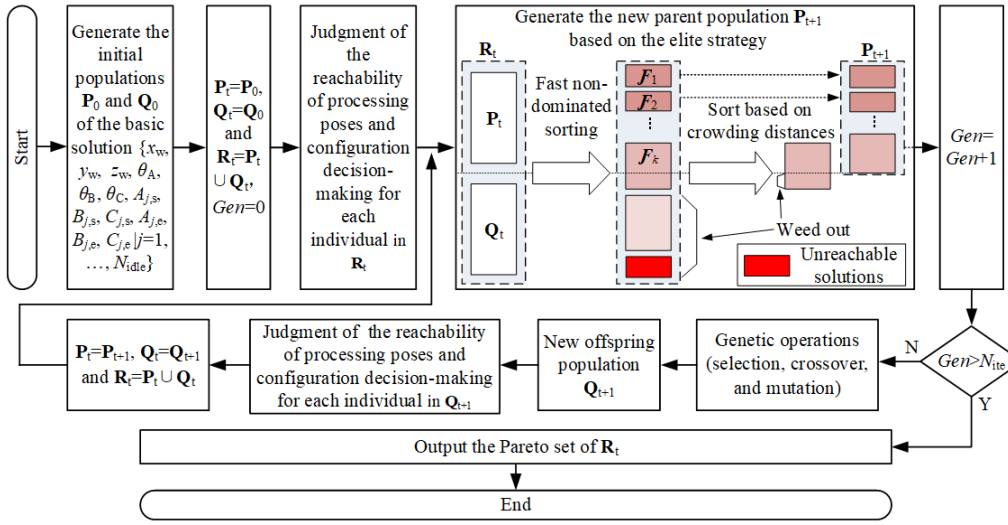

Fig. 3. The integrated optimization process based on the NSGA-II algorithm

4. Case study

In the section, a case study is conducted in detail to evaluate the energy-saving potential of robot laser welding systems and verify the effectiveness of the proposed methods.

4.1. Case introduction

The workpiece is a bicycle frame. The processing platform is the robot laser welding system used in [20], and the welding process parameters is: laser power of 2.75 kW, welding speed of 3 m/min (50 mm/s), and defocusing distance of 0 mm. Fig. 4 shows the three-dimensional model of the bicycle frame and the sub-motions corresponding to a welding process selected. The welding process selected has 12 idle sub-motions and 11 welding sub-motions. The idle sub-motions and welding sub-motions are alternating and the sequence is shown in Fig. 4. The path lengths of welding sub-motion □1 to □11 are 19.70 mm, 58.74 mm, 22.20 mm, 62.02 mm, 52.98 mm, 61.11 mm, 33.60 mm, 31.98 mm, 23.69 mm, 37.60 mm, and 34.80 mm, respectively. The idle sub-motions, which are represented by the number with a circle, adopt the point-to-point motion.

By analyzing the characteristics of the selected welding process, the following knowledges can be easily obtained. Considering the fixed configuration of robots at the Home position, only the laser tool orientation and inverse kinematic solution at the end-point need to be taken into account for the initial idle sub-motion, while only the laser tool orientation and inverse kinematic solution at the start-point need to be taken into account for the final idle sub-motion. The laser tool orientation and the selection of eight inverse kinematic solutions at the start-point of the subsequent sub-motion are consistent with those at the end-point of the preceding sub-motion. It is necessary for all target points in continuous path motion to select the inverse kinematic solution with the same index, to ensure continuous motion along the specified path. Consequently, only one variable, which indicates the selection of inverse kinematic solutions at the start-point is required for continuous path motion. The orientation of the laser tool axis keeps the value

predetermined along the whole trace of the tool centre point for a welding sub-motion, and therefore the attitude angle B and C of the laser tool in $\{CS_W\}$ are constant.

Therefore, the basic solution is $\{x_w, y_w, z_w, \theta_A, \theta_B, \theta_C, A_{1,e}, A_{2,s}, A_{2,e}, A_{3,s}, A_{3,e}, A_{4,s}, A_{4,e}, A_{5,s}, A_{5,e}, A_{6,s}, A_{6,e}, A_{7,s}, A_{7,e}, A_{8,s}, A_{8,e}, A_{9,s}, A_{9,e}, A_{10,s}, A_{10,e}, A_{11,s}, A_{11,e}, A_{12,s}\}$ and the subordinate solution is $\{cf_{1,e}, cf_{2,e}, cf_{3,e}, cf_{4,e}, cf_{5,e}, cf_{6,e}, cf_{7,e}, cf_{8,e}, cf_{9,e}, cf_{10,e}, cf_{11,e}\}$ for the problem corresponding to the welding process selected of the bicycle frame. The values of attitude angles B and C are determined by the value of the attitude angle A and the orientation of the laser tool axis planned. The value range of each decision variable in the basic solution is shown in Table 1.

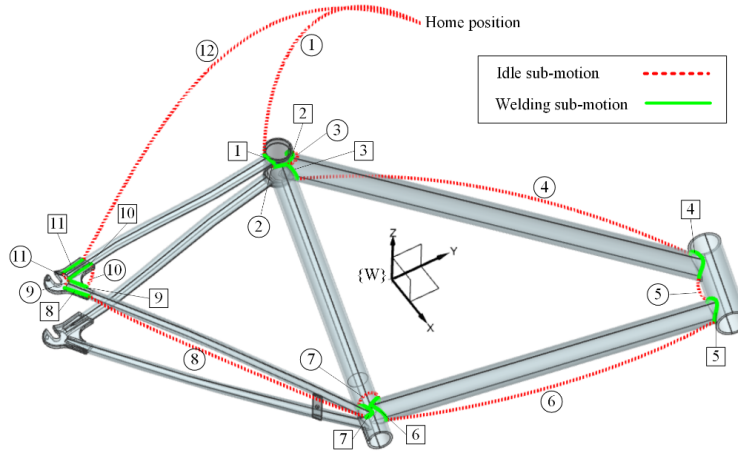

Fig. 4. The bicycle frame model and welding paths

Table 1. The value ranges of decision variables

Decision variables	Value ranges	Decision variables	Value ranges	Decision variables	Value ranges	Decision variables	Value ranges
x_w (mm)	[970, 1940]	$A_{2,s}$ (°)	[–100, 100]	$A_{5,e}$ (°)	[–100, 100]	$A_{9,s}$ (°)	[–100, 100]
y_w (mm)	[–1300, 1300]	$A_{2,e}$ (°)	[–100, 100]	$A_{6,s}$ (°)	[–100, 100]	$A_{9,e}$ (°)	[–100, 100]
z_w (mm)	[0, 2300]	$A_{3,s}$ (°)	[–100, 100]	$A_{6,e}$ (°)	[–100, 100]	$A_{10,s}$ (°)	[–100, 100]
θ_A (°)	[–150, 150]	$A_{3,e}$ (°)	[–100, 100]	$A_{7,s}$ (°)	[–100, 100]	$A_{10,e}$ (°)	[–100, 100]
θ_B (°)	[–100, 100]	$A_{4,s}$ (°)	[–100, 100]	$A_{7,e}$ (°)	[–100, 100]	$A_{11,s}$ (°)	[–100, 100]
θ_C (°)	[–100, 100]	$A_{4,e}$ (°)	[–100, 100]	$A_{8,s}$ (°)	[–100, 100]	$A_{11,e}$ (°)	[–100, 100]
$A_{1,e}$ (°)	[–100, 100]	$A_{5,s}$ (°)	[–100, 100]	$A_{8,e}$ (°)	[–100, 100]	$A_{12,s}$ (°)	[–100, 100]

Table 2. The original scheme

x_w (mm)	y_w (mm)	z_w (mm)	θ_A (°)	θ_B (°)	θ_C (°)	$A_{1,e}$ (°)	$A_{2,s}$ (°)	$A_{2,e}$ (°)	$A_{3,s}$ (°)
1420	0	800	10	0	0	0	0	0	0
$A_{3,e}$ (°)	$A_{4,s}$ (°)	$A_{4,e}$ (°)	$A_{5,s}$ (°)	$A_{5,e}$ (°)	$A_{6,s}$ (°)	$A_{6,e}$ (°)	$A_{7,s}$ (°)	$A_{7,e}$ (°)	$A_{8,s}$ (°)
0	0	0	0	0	0	0	0	0	0
$A_{8,e}$ (°)	$A_{9,s}$ (°)	$A_{9,e}$ (°)	$A_{10,s}$ (°)	$A_{10,e}$ (°)	$A_{11,s}$ (°)	$A_{11,e}$ (°)	$A_{12,s}$ (°)	$cf_{1,e}$	$cf_{2,e}$
0	0	0	0	0	0	0	0	#7	#7
$cf_{3,e}$	$cf_{4,e}$	$cf_{5,e}$	$cf_{6,e}$	$cf_{7,e}$	$cf_{8,e}$	$cf_{9,e}$	$cf_{10,e}$	$cf_{11,e}$	–
#7	#7	#7	#7	#7	#7	#7	#7	#7	–

In general, the workers mainly focus on the accessibility of the processing posture, the singularity of robotic configurations, the continuity of continuous path motion, and collision avoidance. The relevant decision variables of the original scheme are determined according to the general principle. Usually, the workpiece is installed in the middle of the robot workspace to achieve maximum processing flexibility. According to the principle of no bias, the attitude angles

of the laser tool at the starting and ending points of each sub-motion are all taken as zero based on the corresponding value ranges in Table 1. Under the layout pose of the bicycle frame and laser tool postures aforementioned, except for the start-point of the first idle sub-motion and the end-point of the final idle sub-motion, the #7 inverse kinematic solution is selected at other starting and ending points of sub-motions, to achieve the minimum change in joint position relative to Home position. Table 2 shows the decision variable values corresponding to the original scheme.

4.2. Results and analysis

The independent optimization and integrated optimization of three factors: the workpiece layout pose, the laser tool posture, and the inverse kinematics solution are performed. In all optimizations, the population size is $N_{\mathrm{P}} = 100$, the crossover probability is 0.7, the mutation probability is 0.2. All optimization calculations are performed in the MATLAB software on a computer with an Intel i3-8100 CPU 3.60 GHz and 8-GB DDR2. In the following text, to simplify the expression, $Pose_{\mathrm{W}}$ is used to represent the workpiece layout pose, $Posture_{\mathrm{tool}}$ is used to represent the laser tool posture, and IKS is used to represent the inverse kinematics solution.

4.2.1. Independent optimization of $Pose_{\mathrm{W}}$, $Posture_{\mathrm{tool}}$, and IKS

To demonstrate the impact of three factors: $Pose_{\mathrm{W}}$, $Posture_{\mathrm{tool}}$, and IKS on the energy consumption and excution time of idle sub-motions, the independent optimization of each factor is carried out with the optimization order of $Pose_{\mathrm{W}} \rightarrow Posture_{\mathrm{tool}} \rightarrow IKS$. The maximum iteration number is 200 for the optimization of each factor. Two types of optimization situations are considered, as shown in Table 3.

Table 3. Two optimization situations

Optimization order	Optimization situation I			Optimization situation II		
	$Pose_{\mathrm{W}}$	$Posture_{\mathrm{tool}}$	IKS	$Pose_{\mathrm{W}}$	$Posture_{\mathrm{tool}}$	IKS
First	Optimizing	Original scheme	Original scheme	Optimizing	Original scheme	Original scheme
Second	Original scheme	Optimizing	Original scheme	Optimized scheme	Optimizing	Original scheme
Third	Original scheme	Original scheme	Optimizing	Optimized scheme	Optimized scheme	Optimizing

Furthermore, we conducted a single-objective optimization with using energy consumption as the cost function under identical conditions. During this procedure, we adopted a genetic algorithm which incorporates an elitism preservation strategy. Table 4 provides a comparative analysis of the results and computational efficiency between the energy consumption-based single-objective optimization and the multi-objective optimization proposed. E^*_{min} is the energy consumption of the best individual obtained by the optimization, and T^* is the execution time corresponding to E^*_{min}.

According to the data presented in Table 4, compared to the single-objective optimization focused on energy consumption, the multi-objective optimization method proposed achieves a significant reduction in optimization computation time, exceeding 95 %. Furthermore, it yields remarkably similar optimization results, exhibiting deviations of less than 1.5 %. Additionally, it is essential to exhibit the correlation characteristics between the three feature targets and energy consumption. When each of the three feature objectives f_{t}, f_{θ}, and $f_{\dot{\mathrm{q}}}$ and the energy consumption objective is minimum or maximum, the results of the corresponding Pareto-optimal solution, which is obtained by the optimization of $Pose_{\mathrm{W}}$, are shown in Table 5.

According to the data in Table 5, we observe that the minima of any one of three feature objectives do not align with the minimum energy consumption scenario. This suggests a coupled relationship among these feature objectives and energy consumption. Specifically, the fluctuation

in energy consumption is not solely determined by the variation in a single feature objective; it is also impacted by the degree of change in the other two feature objectives. In summary, among the three feature objectives examined, f_{t} exhibits the most substantial impact on energy consumption, followed by f_{θ}, while $f_{\dot{\mathrm{q}}}$ has a comparably smaller influence. The results suggest that the selection of these three feature objectives is appropriate, and they can collectively function as cost functions for assessing energy consumption. The solving approach proposed is reliable for the energy consumption optimization problem.

Table 4. A comparison of results and computational efficiency between the single-objective optimization and the multi-objective optimization proposed

		Optimization situation I			Optimization situation II		
		$Pose_{\mathrm{W}}$	$Posture_{\mathrm{tool}}$	IKS	$Pose_{\mathrm{W}}$	$Posture_{\mathrm{tool}}$	IKS
Single-objective optimization	Computation time (min)	635.57	717.38	951.20	635.57	779.16	844.62
	$E^*_{\min}$ (J)	29075.84	29445.11	37948.05	29075.84	27630.73	26497.63
	T^* (s)	4.31	4.38	5.46	4.31	4.16	4.03
Multi-objective optimization proposed	Computation time (min)	26.85	22.14	7.94	26.85	22.75	3.89
	$E^*_{\min}$ (J)	29239.43	29753.34	38497.56	29239.43	27486.89	26601.83
	T^* (s)	4.33	4.43	5.54	4.33	4.13	4.05
Deviation in computational time		–95.78 %	–96.91 %	–99.16 %	–95.78 %	–97.08 %	–99.54 %
Deviation in energy consumption		0.56 %	1.04 %	1.45 %	0.56 %	–0.52 %	0.39 %
Note: The deviation = (Multi-objective optimization value - Single-objective optimization value)/Single-objective optimization value *100 %							

Table 5. Corresponding results for minimum and maximum of each objective, respectively

Category	f_{t} (s)	f_{θ} (°)	$f_{\dot{\mathrm{q}}}$ (°/s)	Energy consumption (J)
Minimum f_{t}	4.12	159.30	53.08	32728.18
Maximum f_{t}	5.36	141.80	27.27	35436.97
Minimum f_{θ}	4.62	119.71	39.30	30110.89
Maximum f_{θ}	4.12	159.53	52.57	32707.60
Minimum $f_{\dot{\mathrm{q}}}$	5.36	141.80	27.27	35436.97
Maximum $f_{\dot{\mathrm{q}}}$	4.12	158.91	53.21	32662.03
Minimum energy consumption	4.33	127.58	41.30	29239.43
Maximum energy consumption	5.36	141.80	27.27	35436.97
Original scheme	6.00	188.38	41.82	41242.79

To illustrate the influence of three factors on energy consumption, Figs. 5-6 show the Pareto-optimal solutions obtained by the optimization of three factors and the corresponding energy consumption simulation values for the optimization situation I and II, respectively. N_{Pareto} is the number of Pareto-optimal solutions. E_{idle} represents the total energy consumption of idle sub-motions.

According to the results in Figs. 5-6, each of the three factors $Pose_{\mathrm{W}}$, $Posture_{\mathrm{tool}}$, and IKS has a significant impact on the energy consumption and execution time of idle sub-motions. The effect of optimizing multiple factors is better than that of optimizing a single factor. Compared to only optimizing one of $Pose_{\mathrm{W}}$, $Posture_{\mathrm{tool}}$, and IKS, the optimizition of all three factors leads to reductions in energy consumption by 9.02 %, 10.59 %, and 30.90 %, respectively. Notably, the optimization effects of $Posture_{\mathrm{tool}}$ and IKS considerably differ for different $Pose_{\mathrm{W}}$ or $Posture_{\mathrm{tool}}$. The significant variance suggests that $Pose_{\mathrm{W}}$, $Posture_{\mathrm{tool}}$, and IKS are interconnected and mutually dependent. Therefore, it is imperative to consider the combined influence of $Pose_{\mathrm{W}}$, $Posture_{\mathrm{tool}}$, and IKS.

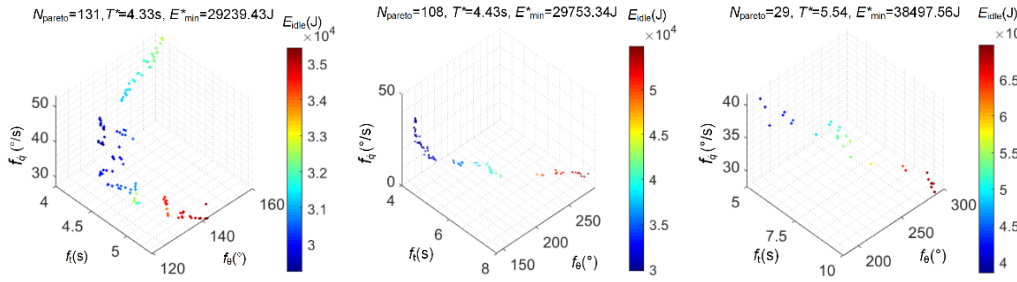

a) The optimization of workpiece layout poses

b) The optimization of laser tool postures

c) The optimization of inverse kinematics solutions

Fig. 5. The Pareto-optimal solutions obtained and the corresponding energy consumption simulation values for the optimization situation I

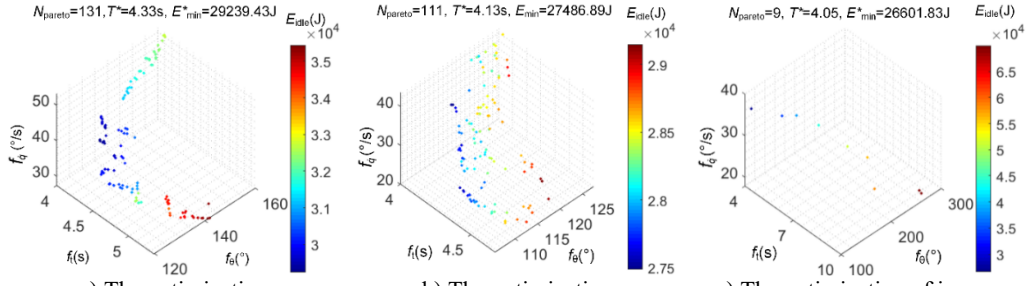

a) The optimization of workpiece layout poses

b) The optimization of laser tool postures

c) The optimization of inverse kinematics solutions

Fig. 6. The Pareto-optimal solutions obtained and the corresponding energy consumption simulation values for the optimization situation II

4.2.2. Integrated optimization of $Pose_{\mathrm{W}}$, $Posture_{\mathrm{tool}}$, and IKS

For the independent optimization of three factors, the coupling impact of three factors on the optimization results is not considered. Therefore, we also do the integrated optimization of $Pose_{\mathrm{W}}$, $Posture_{\mathrm{tool}}$, and IKS from a random initial population. In order to ensure that the iteration number of the basic solutions for two ways are basically the same, the maximum iteration number for the integrated optimization is 400. Fig. 7 shows the Pareto-optimal solutions obtained after 10, 200, and 400 iterations and the corresponding energy consumption simulation values.

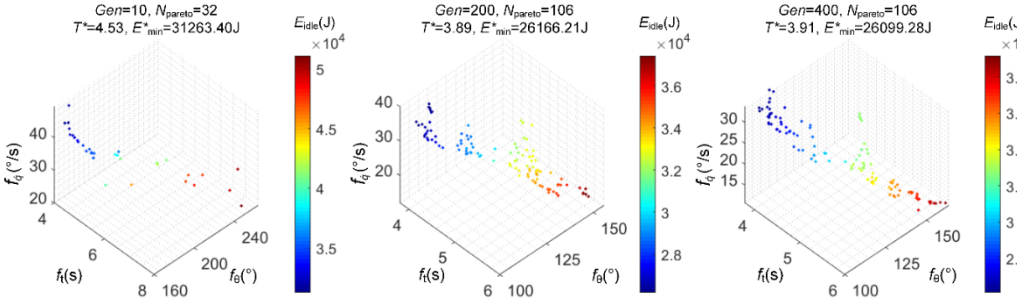

Fig. 7. The Pareto-optimal solutions obtained by the integrated optimization and the corresponding energy consumption simulation values

According to the results in Fig. 7, with the search proceeding, the individuals in the population move towards the Pareto-optimal region in total, the minimum energy consumption gradually decreases, and the non-dominated points corresponding to the Pareto-optimal solutions found are well distributed in the objective vector space. The difference between two minimum energy

consumption values found through 200 and 400 iterations is small (about 66.93 J), and the two minimum energy consumption values are smaller than the minimum energy consumption obtained by the independent optimization of three factors for the optimization situation II (reduced by 435.62 J and 502.55 J, respectively). It indicates that the proposed integrated optimization process based on the NSGA-II algorithm is applicable, and the energy-saving effect of integrated optimization, which considers the coupling among $Pose_{\mathrm{W}}$, $Posture_{\mathrm{tool}}$, and IKS, is better than that of the independent optimization.

Table 6. The best Pareto scheme searched

x_{W} (mm)	y_{W} (mm)	z_{W} (mm)	θ_{A} (°)	θ_{B} (°)	θ_{C} (°)	$A_{1,\mathrm{e}}$ (°)	$A_{2,\mathrm{s}}$ (°)	$A_{2,\mathrm{e}}$ (°)	$A_{3,\mathrm{s}}$ (°)
1136.28	112.68	1062.33	32.02	45.62	33.775	17.22	18	14	32
$A_{3,\mathrm{e}}$ (°)	$A_{4,\mathrm{s}}$ (°)	$A_{4,\mathrm{e}}$ (°)	$A_{5,\mathrm{s}}$ (°)	$A_{5,\mathrm{e}}$ (°)	$A_{6,\mathrm{s}}$ (°)	$A_{6,\mathrm{e}}$ (°)	$A_{7,\mathrm{s}}$ (°)	$A_{7,\mathrm{e}}$ (°)	$A_{8,\mathrm{s}}$ (°)
36	–72.44	4	28	10	18	32	4	8	14
$A_{8,\mathrm{e}}$ (°)	$A_{9,\mathrm{s}}$ (°)	$A_{9,\mathrm{e}}$ (°)	$A_{10,\mathrm{s}}$ (°)	$A_{10,\mathrm{e}}$ (°)	$A_{11,\mathrm{s}}$ (°)	$A_{11,\mathrm{e}}$ (°)	$A_{12,\mathrm{s}}$ (°)	$cf_{1,\mathrm{e}}$	$cf_{2,\mathrm{e}}$
8	20	14	32	32	16	22	–16	#3	#3
$cf_{3,\mathrm{e}}$	$cf_{4,\mathrm{e}}$	$cf_{5,\mathrm{e}}$	$cf_{6,\mathrm{e}}$	$cf_{7,\mathrm{e}}$	$cf_{8,\mathrm{e}}$	$cf_{9,\mathrm{e}}$	$cf_{10,\mathrm{e}}$	$cf_{11,\mathrm{e}}$	–
#3	#3	#3	#3	#3	#3	#3	#3	#3	–

Table 6 shows the decision variable values corresponding to the best solution scheme found. The KUKA KR60-3 robot is used to carry out the motion experiments of the original scheme and the best solution scheme, and the execution time and robotic energy consumption data were measured. The energy consumption of the laser and the chiller is calculated based on the execution time measured. The statistical average of multiple measurement results is used for relevant calculations, to reduce the impact of measurement errors on the final results. The comparisons of processing energy consumption and execution time between the two schemes are illustrated in Fig. 8. The rectangular bar represents the sample mean of each parameter, and the red line represents the confidence interval of each parameter calculated at a 95 % confidence level.

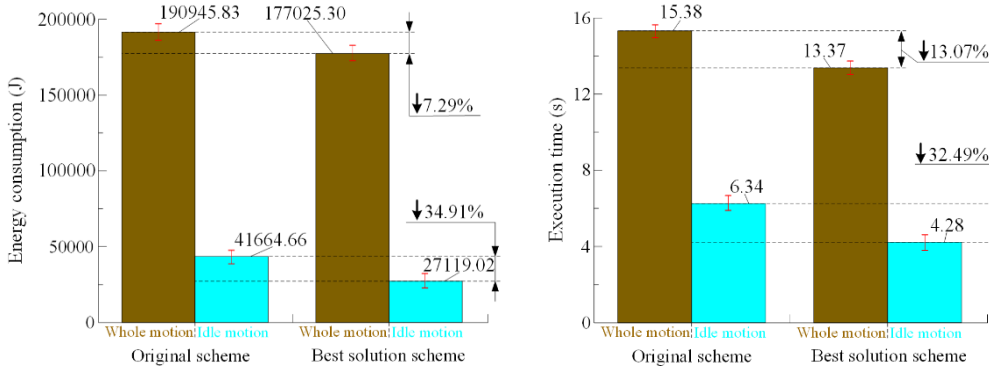

a) Comparison of energy consumption b) Comparison of execution time

Fig. 8. Processing energy consumption and execution time of two schemes

According to the results in Table 2, Table 6, and Fig. 8, there is a significant difference in $Pose_{\mathrm{W}}$ and $Posture_{\mathrm{tool}}$ between two schemes. Compared with the original scheme, the best solution scheme reduces the energy consumption and execution time of idle sub-motions by 34.91 % and 32.49 %, respectively, while the total energy consumption and execution time of the whole motion are reduced by 7.29 % and 13.07 %, respectively. The results show that the robot laser welding of complex components has great potential in energy conservation. In addition, due to the complexity of robot kinematics characteristics and energy consumption characteristics, there is a large optimization space in energy efficiency and efficiency for the processing scheme which is planned by operators based on the general cognition. Therefore, the optimization operation is necessary.

5. Conclusions

This study concentrates on the energy-saving optimization methods of robotic laser welding of complex components, to address the challenges of high energy consumption and low energy efficiency. By analyzing the kinematic characteristics of 6-axis robots and the energy consumption characteristics of robot laser welding systems, it is evident that three factors: the layout pose of workpieces, the posture of laser tools, and the inverse kinematics solution substantially impact the optimal energy consumption and the corresponding execution time for robot laser welding systems performing a task. Therefore, it is crucial to optimize these factors, to enhance processing efficiency and energy utilization.

The findings from the case study demonstrate the feasibility and efficacy of the proposed energy-saving method and problem-solving approach. Robot laser welding of complex components exhibits considerable potential for energy conservation in appropriate scenarios. Optimizing the layout pose of workpieces, the posture of laser tools, and the inverse kinematics solutions is an effective strategy for reducing energy consumption in the processing of complex components. In the case study, compared to the original scheme, the best solution scheme achieves a reduction of 34.91 % in energy consumption and a 32.49 % reduction in execution time for idle sub-motions, while decreasing total energy consumption by 7.29 % and overall execution time by 13.07 %.

The proposed method can be extended to optimize energy consumption in other robotic processing systems. Furthermore, applying the proposed method to optimize the multi-robot collaborative processing holds significant practical value in relevant scenarios. Furthermore, the development of efficient solution methods for minimizing energy consumption remains a highly significant research area.

Acknowledgements

The authors appreciate the supports of the Science and Technology Research Program of Chongqing Municipal Education Commission in China, grant number KJQN202303422, the Natural Science Foundation of Chongqing in China, grant number 2022NSCQMSX1629, and the 2022 China University Innovation Fund - Beichuang Teaching Assistant project, grant number 2021BCB02008.

Data availability

The datasets generated during and/or analyzed during the current study are available from the corresponding author on reasonable request.

Author contributions

Jin Zhou: conceptualization, methodology, investigation, software, writing-original draft preparation, and funding acquisition. Pei Jiang: refining the ideas, writing-review and editing, and funding acquisition. Chongfu Huang: supervision, writing-review and editing, and funding acquisition. Kehan Ping: visualization.

Conflict of interest

The authors declare that they have no conflict of interest.

References

[1] X. Wang, X. Zhou, Z. Xia, and X. Gu, "A survey of welding robot intelligent path optimization," *Journal of Manufacturing Processes*, Vol. 63, pp. 14–23, Mar. 2021, https://doi.org/10.1016/j.jmapro.2020.04.085

[2] C. Lv, L. Zou, Y. Huang, H. Li, T. Wang, and Y. Mu, "A novel toolpath for robotic adaptive grinding of extremely thin blade edge based on dwell time model," *IEEE/ASME Transactions on Mechatronics*, Vol. 27, No. 6, pp. 4429–4439, Dec. 2022, https://doi.org/10.1109/tmech.2022.3156804

[3] "Executive summary world robotics 2022 industrial robots," IFR, 2022.

[4] M. Gadaleta, M. Pellicciari, and G. Berselli, "Optimization of the energy consumption of industrial robots for automatic code generation," *Robotics and Computer-Integrated Manufacturing*, Vol. 57, pp. 452–464, Jun. 2019, https://doi.org/10.1016/j.rcim.2018.12.020

[5] I. Palomares et al., "A panoramic view and swot analysis of artificial intelligence for achieving the sustainable development goals by 2030: progress and prospects," *Applied Intelligence*, Vol. 51, No. 9, pp. 6497–6527, Jun. 2021, https://doi.org/10.1007/s10489-021-02264-y

[6] G. Notomista et al., "A resilient and energy-aware task allocation framework for heterogeneous multirobot systems," *IEEE Transactions on Robotics*, Vol. 38, No. 1, pp. 159–179, Feb. 2022, https://doi.org/10.1109/tro.2021.3102379

[7] D. Meike, M. Pellicciari, and G. Berselli, "Energy efficient use of multirobot production lines in the automotive industry: detailed system modeling and optimization," *IEEE Transactions on Automation Science and Engineering*, Vol. 11, No. 3, pp. 798–809, Jul. 2014, https://doi.org/10.1109/tase.2013.2285813

[8] M. Zhang and J. Yan, "A data-driven method for optimizing the energy consumption of industrial robots," *Journal of Cleaner Production*, Vol. 285, p. 124862, Feb. 2021, https://doi.org/10.1016/j.jclepro.2020.124862

[9] M. Gadaleta, G. Berselli, M. Pellicciari, and F. Grassia, "Extensive experimental investigation for the optimization of the energy consumption of a high payload industrial robot with open research dataset," *Robotics and Computer-Integrated Manufacturing*, Vol. 68, p. 102046, Apr. 2021, https://doi.org/10.1016/j.rcim.2020.102046

[10] P. Jiang, Z. Wang, X. Li, X. V. Wang, B. Yang, and J. Zheng, "Energy consumption prediction and optimization of industrial robots based on LSTM," *Journal of Manufacturing Systems*, Vol. 70, pp. 137–148, Oct. 2023, https://doi.org/10.1016/j.jmsy.2023.07.009

[11] G. Carabin, E. Wehrle, and R. Vidoni, "A review on energy-saving optimization methods for robotic and automatic systems," *Robotics*, Vol. 6, No. 4, p. 39, Dec. 2017, https://doi.org/10.3390/robotics6040039

[12] A. Vergnano et al., "Embedding detailed robot energy optimization into high-level scheduling," in *IEEE International Conference on Automation Science and Engineering (CASE 2010)*, p. 38339, Aug. 2010, https://doi.org/10.1109/coase.2010.5584686

[13] O. Wigstrom, B. Lennartson, A. Vergnano, and C. Breitholtz, "High-level scheduling of energy optimal trajectories," *IEEE Transactions on Automation Science and Engineering*, Vol. 10, No. 1, pp. 57–64, Jan. 2013, https://doi.org/10.1109/tase.2012.2198816

[14] H. Cao, J. Zhou, P. Jiang, K. K. B. Hon, H. Yi, and C. Dong, "An integrated processing energy modeling and optimization of automated robotic polishing system," *Robotics and Computer-Integrated Manufacturing*, Vol. 65, p. 101973, Oct. 2020, https://doi.org/10.1016/j.rcim.2020.101973

[15] X. Li, Y. Lan, P. Jiang, H. Cao, and J. Zhou, "An efficient computation for energy optimization of robot trajectory," *IEEE Transactions on Industrial Electronics*, Vol. 69, No. 11, pp. 11436–11446, Nov. 2022, https://doi.org/10.1109/tie.2021.3118367

[16] F. Merlo, G. Vazzoler, and G. Berselli, "Eco-programming of industrial robots for sustainable manufacturing via dynamic time scaling of trajectories," *Robotics and Computer-Integrated Manufacturing*, Vol. 79, p. 102420, Feb. 2023, https://doi.org/10.1016/j.rcim.2022.102420

[17] M. Gadaleta, G. Berselli, and M. Pellicciari, "Energy-optimal layout design of robotic work cells: Potential assessment on an industrial case study," *Robotics and Computer-Integrated Manufacturing*, Vol. 47, pp. 102–111, Oct. 2017, https://doi.org/10.1016/j.rcim.2016.10.002

[18] Y. Feng, Z. Ji, Y. Gao, H. Zheng, and J. Tan, "An energy-saving optimization method for cyclic pick-and-place tasks based on flexible joint configurations," *Robotics and Computer-Integrated Manufacturing*, Vol. 67, p. 102037, Feb. 2021, https://doi.org/10.1016/j.rcim.2020.102037

[19] E. Uhlmann, S. Reinkober, and T. Hollerbach, "Energy efficient usage of industrial robots for machining processes," *Procedia CIRP*, Vol. 48, pp. 206–211, Jan. 2016, https://doi.org/10.1016/j.procir.2016.03.241

[20] J. Zhou, H. Yi, H. Cao, P. Jiang, C. Zhang, and W. Ge, "Structural decomposition-based energy consumption modeling of robot laser processing systems and energy-efficient analysis," *Robotics and*

Computer-Integrated Manufacturing, Vol. 76, p. 102327, Aug. 2022, https://doi.org/10.1016/j.rcim.2022.102327

[21] M. Schmitz, F. Pinsker, A. Ruhri, B. Jiang, and G. Safronov, "Enabling rewards for reinforcement learning in laser beam welding processes through deep learning," in *19th IEEE International Conference on Machine Learning and Applications (ICMLA)*, pp. 1424–1431, Dec. 2020, https://doi.org/10.1109/icmla51294.2020.00221

[22] J. Bremer, P. Walderich, N. Pirch, J. H. Schleifenbaum, A. Gasser, and T. Schopphoven, "Effects of path accuracy on additively manufactured specimens by laser material deposition using six-axis robots," *Journal of Laser Applications*, Vol. 33, No. 1, Feb. 2021, https://doi.org/10.2351/7.0000308

[23] Y. Wang, P. Jiang, J. Zhao, S. Geng, and B. Xu, "Effects of energy density attenuation on the stability of keyhole and molten pool during deep penetration laser welding process: A combined numerical and experimental study," *International Journal of Heat and Mass Transfer*, Vol. 176, p. 121410, Sep. 2021, https://doi.org/10.1016/j.ijheatmasstransfer.2021.121410

[24] S. M. H. Hojjatzadeh et al., "Direct observation of pore formation mechanisms during LPBF additive manufacturing process and high energy density laser welding," *International Journal of Machine Tools and Manufacture*, Vol. 153, p. 103555, Jun. 2020, https://doi.org/10.1016/j.ijmachtools.2020.103555

[25] M. Tavana, M. Soltanifar, F. J. Santos-Arteaga, and H. Sharafi, "Analytic hierarchy process and data envelopment analysis: A match made in heaven," *Expert Systems with Applications*, Vol. 223, p. 119902, Aug. 2023, https://doi.org/10.1016/j.eswa.2023.119902

[26] K. Deb, A. Pratap, S. Agarwal, and T. Meyarivan, "A fast and elitist multiobjective genetic algorithm: NSGA-II," *IEEE Transactions on Evolutionary Computation*, Vol. 6, No. 2, pp. 182–197, Apr. 2002, https://doi.org/10.1109/4235.996017

Jin Zhou received Ph.D. degree in mechanical engineering from Chongqing University, Chongqing, China, in 2022. He is currently a Lecturer at Chongqing Vocational Institute of Engineering. His current research interests include robotic kinematics, dynamics and control, energy consumption modeling of manufacturing systems, energy-saving methods of robotic systems, and robotic trajectory planning methods.

Pei Jiang received Ph.D. degree in control science and engineering from the Zhejiang University, Zhejiang, China in 2015, respectively. He is currently an Associate Professor at College of Mechanical Engineering, Chongqing University, Chongqing, China. His research interests include robotic systems, soft robotics, and energy modeling of industrial robots.

Chongfu Huang received B.S. degree in electrical engineering and automation from Liaoning Technical University, Liaoning, China, in 1996. He is currently an Associate Professor at Chongqing Vocational Institute of Engineering. His current research interests include control, optimization technique, and intelligent manufacturing.

Kehan Ping received M.S. degree in Mechanical Engineering from Chongqing University, Chongqing, China, in 2024. Now he works at Huagong Central Academy of Science and Technology. His current research interests include robotic systems and energy modeling of industrial robots.